Prostate cancer detection from model-free T1-weighted time series and diffusion imaging

Nandinee Fariah Haq[a], Piotr Kozlowski[b,c], Edward C. Jones[d],
Silvia D. Chang[c], S. Larry Goldenberg[b], Mehdi Moradi[e]

[a]Departments of Electrical and Computer Engineering; [b]Urologic Sciences;
[c]Radiology; [d]Pathology and Molecular Medicine;
University of British Columbia, Vancouver, BC, Canada,
[e] IBM Almaden Research Center, San Jose, CA.

ABSTRACT

The combination of Dynamic Contrast Enhanced (DCE) images with diffusion MRI has shown great potential in prostate cancer detection. The parameterization of DCE images to generate cancer markers is traditionally performed based on pharmacokinetic modeling. However, pharmacokinetic models make simplistic assumptions about the tissue perfusion process, require the knowledge of contrast agent concentration in a major artery, and the modeling process is sensitive to noise and fitting instabilities. We address this issue by extracting features directly from the DCE T1-weighted time course without modeling. In this work, we employed a set of data-driven features generated by mapping the DCE T1 time course to its principal component space, along with diffusion MRI features to detect prostate cancer. The optimal set of DCE features is extracted with sparse regularized regression through a Least Absolute Shrinkage and Selection Operator (LASSO) model. We show that when our proposed features are used within the multiparametric MRI protocol to replace the pharmacokinetic parameters, the area under ROC curve is 0.91 for peripheral zone classification and 0.87 for whole gland classification. We were able to correctly classify 32 out of 35 peripheral tumor areas identified in the data when the proposed features were used with support vector machine classification. The proposed feature set was used to generate cancer likelihood maps for the prostate gland.

Keywords: Multiparametric magnetic resonance imaging, principal component analysis, LASSO, SVM.

1. INTRODUCTION

Multiparametric magnetic resonance imaging (mpMRI), where parameters from different MRI modalities are used in combination, is now considered part of the standard of care for image-based evaluation of prostate to determine the need for a biopsy in many parts of the world.[1] Improved accuracy of prostate cancer detection and localization is reported when different MR modalities are used together. Among other modalities, diffusion weighted imaging (DWI) has the ability to characterize the de-phasing of MR signal caused by molecular diffusion. In cancerous regions, the regular tissue distribution pattern in prostate is disturbed and replaced by masses of malignant epithelial cells and glands. This pathological change alters the tissue diffusion pattern in prostate that results in changing parameter values extracted from diffusion MRI.

Diffusion Tensor Imaging (DTI) is an advanced form of DWI that enables the measurement of directionality along with the magnitude of water diffusion. While DWI generates one diffusion parameter, namely Apparent Diffusion Coefficient (ADC), most of the studies on quantitative DTI use two diffusion parameters, namely average diffusivity ($\langle D \rangle$) and Fractional Anisotropy (FA). Average diffusivity is the trace of the diffusion tensor. FA is an indication of how anisotropic the diffusion process is and it can only be extracted from DTI. Decreased ADC and $\langle D \rangle$ values are reported frequently as a strong indicator of tumors.[2–4] Gibbs *et al.*[5] and Wang *et al.*[6] reported an inverse relationship between diffusivity values and tumor proliferation using histological measurements of cellular density. Hambrock *et al.*[7] and Tamada *et al.*[8] reported a negative correlation between

Further author information: Send correspondence to:
N. Haq (nandinee@ece.ubc.ca)

diffusivity values and Gleason grades. However, the association of FA with tumor is indecisive and different studies reported increased,[4] decreased[9] and even unchanged values of FA in prostate carcinoma.[10]

Several studies reported that when quantitative parameters extracted from diffusion MRI and DCE MRI are used together, it results in a better cancer detection accuracy than when used separately.[11,12] Oto *et al.*[13] reported significant increase in sensitivity when K^{trans} is used with average diffusivity values with multivariate logistic regression. Delongchamps *et al.*[14] reported significantly better cancer detection performance in peripheral zone of prostate when DCE and diffusion MRI are used together with T2 compared to when DCE and diffusion MRI are used separately with T2. Langer *et al.* investigated different combinations of parameters from DCE, DTI and T2 and the highest performance in terms of area under Receiver Operating Characteristics curve (ROC) was achieved when $\langle D \rangle$ and K^{trans} were used with T2.[15] In,[16] these three parameters were reported to be significantly correlated with specific histologic components that differ between normal and cancerous peripheral zone of prostate, and hence can be used in combination as an image-based prognostic parameter.

To separate cancer and normal tissues, some studies focused on applying machine learning approaches by classifying multiparametric MRI parameters.[17] Most of these studies reported their performances in terms of area under ROC, sensitivity, specificity and accuracy. In Kozlowski *et al.*,[18] it is reported that the combination of DTI and DCE parameters at 3 Tesla results in improved cancer diagnostic capability in terms of area under ROC. Moradi *et al.*[19] also reported improved performance with DCE and DTI features and generated a single parameter map of cancer likelihood using support vector machine classification .

In this work, we investigated the performance of data-driven DCE features in a multiparametric framework. In Haq *et al.*,[20] we proposed a set of data-driven features generated by principal component analysis of the kinetic curves of DCE T1 time course and reduced its dimensionality by a Least Absolute Shrinkage and Selection Operator (LASSO). In this work, this set of DCE features is used with DTI features extracted from the registered diffusion images for tumour detection using Support Vector Machine (SVM) classification. The method was validated in 16 clinical cases based on wholemount histopathology slides as the reference. Using this computational framework, we show that the proposed approach to parameterization of DCE data can improve the detection of cancer from DCE data within the mpMRI protocol.

2. MATERIALS AND METHODS

2.1 Data Collection Protocols

The data used in this work was obtained in 2010-2011 for a multiparametric MRI study (PI: P. Kozlowski). The study was approved by the Clinical Research Ethics Board of the University of British Columbia and the patients had given their written consent before entering the study. These patients were scheduled for radical prostatectomy and they went through an MRI imaging session before their surgery. The MRI examination was scheduled 3-48 days prior to their surgery date and the mean time between the MRI session and the radical prostatectomy was 14 days for these patients. The patients recruited for this study had not received any form of therapy before their radical prostatectomy. 21 patients underwent the MRI session out of which 5 patient were excluded from DCE MR imaging due to their allergic reaction to the contrast agent. In this work we used MRI data from 16 patients who underwent both DTI and DCE MRI sessions.

2.1.1 MRI Imaging Protocol

MRI examinations were performed on a 3 Tesla MRI scanner (Achieva, Philips Healthcare, Best, The Netherlands) and the signals were acquired with a combination of an endorectal coil (Medrad, Pittsburgh, PA) and a cardiac phased-array coil (Philips Healthcare, Best, The Netherlands). Fast spin-echo T2-weighted images were acquired in the axial and coronal planes using repetition time (TR) of 1851 ms and an effective echo time (TE) of 80 ms with 14 cm field of view (FOV) (284×225 matrix, 3 averages). Each slice was 4 mm thick and there were no gaps between the slices. 12 axial slices were selected from this sequence and used for DCE MRI scans. T2-weighted images were used to identify the anatomical details of the prostate gland to match MR-slices with histology. The majority of the glands were smaller than 48 mm along the slice selection direction.

DCE T1-weighted images were acquired using a three-dimensional T1-weighted spoiled gradient echo-sequence with a field of view of 24 cm (TR/TE = 3.4/1.06 ms, flip angle = 15°, 256×163 matrix, 2 averages). The contrast

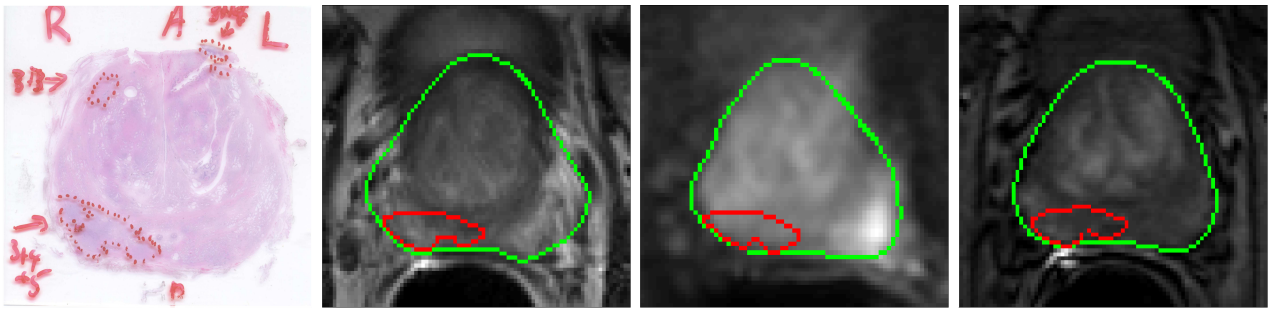

(a) (b) (c) (d)

Figure 1. (a) Peripheral zone tumor of Gleason Grade (3+4+5) from pathology slide is mapped to the corresponding (b) T2-weighted, (c) DTI and (d) DCE-MRI slice. The green contour represents the boundary of the prostate gland and the red contour is the mapped tumor.

agent used here was Gd-DTPA (Magnevist, Berlex Canada) and 0.1 mmol/kg of Gd-DTPA was injected with a motorized power injector within 10 s at the rate of 2 mL/s, followed by a 20 mL flush of saline. To calculate the contrast agent concentration in the prostate, at first proton density (PD) images were acquired (TR/TE = 50/0.95 ms, flip angle = 5°). Subsequently a series of 75 T1-weighted dynamics were acquired, where 3 dynamics were acquired before the injection of the contrast agent, and the remaining 72 dynamics were acquired during and after the injection of the contrast agent. The time resolution was 10.6 s per dynamic and the slice thickness was 4 mm. T1 values were calculated based on PD-weighted and T1-weighted images according to the procedure described by Parker et al.[21] DCE MRI data were processed off-line using Matlab (Mathworks, Natick, MA) and Igor Pro (WaveMetrics, Portland, OR).

DTI data were acquired using a diffusion weighted single shot echo planar imaging (EPI) sequence with a field of view of 24 cm (TR/TE = 2100/74 ms, slice thickness = 4 mm with no gap, 128 × 115 matrix, 6 noncollinear gradient directions, 18 averages, total acquisition time of 8 min, b-value = 0 and 600 s/mm^2). DTI data were processed off-line to calculate fractional anisotropy (FA) and average diffusivity ($\langle D \rangle$) values. Diffusion weighted images were registered to the non-weighted b=0 image with a mutual information algorithm and eigenvalues of the diffusion tensor were calculated. Average diffusivity and fractional anisotropy maps were generated with the proprietary DTI processing toolbox PRIDE (Philips Healthcare, Best, The Netherlands).

2.1.2 Pathology Data

After imaging, patients went through the surgery and radical prostatectomy specimens were acquired. The prostatectomy specimens were dissected and histopathologically examined in a uniform manner to acquire the whole-mount sections. The external surfaces were inked, seminal vesicles were amputated, the apical and bladder neck tissue slices were removed and the specimens were dissected following a minimum of 24-h fixation in 10% buffered formalin. A device described in Drew et al[22] was used to cut the prostate gland from inferior to superior in serial transverse cuts perpendicular to the posterior capsule, at 4 mm intervals, which allowed reasonably good correspondence between the pathology slides and the MR slices.

2.2 Registration

The whole-mount pathology slides are registered with the corresponding T2-weighted, DTI and DCE-MRI images by affine registration followed by B-spline registration. To register the images, prostate region is manually segmented in both pathology images and DCE-MRI slices and registration is applied on the segmented prostate region only. The average Dice similarity coefficient (DSC) value between the pathology and T2-weighted images after registration was 0.93±0.02. The average DSC between T2-weighted and registered DCE image was 0.95±0.03. The same DSC was recorded for T2-weighted to DTI registration. Figure 1 shows one case where the tumor region from the pathology slide is mapped to the corresponding T2-weighted, DTI and DCE MRI slices.

2.3 Feature Extraction and Classification

In this work, we extracted model-free PCA features from DCE-MRI and diffusivity, $\langle D \rangle$ from DTI. To extract the features, the normal and cancer regions were mapped from the wholemount pathology slides to the corresponding DCE and DTI slides and the mapped regions were then used to extract features. Each tumor was taken as a Region Of Interest (ROI) and tumors larger than 100 mm^2 were divided into two or more smaller ROIs.

From the dynamic T1-weighted MR images, the intensity values within each ROI were averaged and an average time course signal was formed. Our approach to data-driven characterization of the DCE time course is to use a dimensionality reduction method to convert the time series of normalized contrast enhanced T1-weighted intensities to an optimally sized vector of features. We used the method described in[20] for this purpose, and extracted the most significant principal components with sparse regularized regression through a Least Absolute Shrinkage and Selection Operator (LASSO) model.

Soft margin Support Vector Machine (SVM) classifier was used to classify cancer and normal tissues with mpMRI feature combination. The margin violation penalty weight, c, and the Radial Basis Function (RBF) kernel parameter, γ, were the two parameters to tune. The classifier was tuned by cross-validation on a leave-one-patient-out basis. We investigated the possible combinations of c and γ by a grid search on $c \in \{2^{-10}, 2^{-9.5}, ..., 2^{10}\}$ and $\gamma \in \{2^{-10}, 2^{-9.5}, ..., 2^{10}\}$, and the cross-validation was targeted at maximizing the AUC.

3. RESULTS

Correlation of the proposed DCE features with traditional pharmacokinetic features: Our PCA-LASSO approach to feature extraction from DCE data provides for model-free parameterization. In this work we investigated the association of these PCA parameters with the pharmacokinetic parameters in the peripheral zone to understand the potential physical meaning of the PCA features. Figure 2 shows the correlation coefficients of PC parameters with pharmacokinetic parameters. For each pharmacokinetic parameter, we have plotted the values and reported the correlation with the top five PCA features in terms of correlation with that specific pharmacokinetic parameter. The second principal component showed maximum correlation with K^{trans} and the calculated linear correlation coefficient (ρ) was -0.70. The first principal component showed the maximum correlation with v_e ($\rho = 0.53$) and the second principal component showed maximum correlation with v_p ($\rho = -0.57$). It is interesting that the first and the second PCA features show maximum correlation with K^{trans} which has consistently performed as the most effective pharmacokinetic parameter in our previous work. This shows that the PCA features effectively capture the disease-related information of the T1 time series.

Cancer detection in the peripheral zone: At first, we investigated the performance of the data-driven mpMRI features in the peripheral zone only. We used 191 regions of interest from the peripheral zone of 16 patients to train and test the classifier. Out of these samples, 92 were from cancer regions and the remaining 99 were from normal areas. The classifier trained on traditional multiparamteric features, i.e. $\langle D \rangle$ and FA from DTI and K^{trans}, v_e and v_p from DCE MRI, generated an AUC of 0.80. At the optimal threshold of 0.24, the sensitivity and specificity was 73.9% and 73.7% respectively. When the classifier was trained on the LASSO-isolated PCA features along with $\langle D \rangle$ from diffusion MRI, the area under ROC was 0.91. The number of LASSO-isolated PCA features to be used in the analysis was determined by forward search algorithm targeted to maximize the AUC. The sensitivity, specificity and accuracy was 85.9%, 80.8% and 83.2% respectively. The slice-level sensitivity was defined as the percent of cases where the classifier can detect more than 50% of the total tumor area. In 32 out of 35 slides, the classifier detected more that 50% area of the tumor, resulting in a slice-level sensitivity of 91.4%. Despite the large increase in AUC from traditional mpMRI to our diffusion plus PCA-LASSO features (from 0.8 to 0.91), the increase was not statistically significant due to small sample size.

Cancer detection in the whole gland: We also investigated the performance of the proposed data-driven mpMRI feature combination in detecting cancer from the entire prostate gland. We extracted 111 regions of interest (43 tumor, 68 normal) from the central gland, and combined these samples with the peripheral zone samples. With traditional multiparametric features, the AUC over 16 patients was 0.68. When the proposed LASSO-isolated PCA features were used with $\langle D \rangle$, the AUC was 0.87. At the optimal threshold of 0.5, the sensitivity, specificity and accuracy were 80.7%, 82.0% and 81.5% respectively. In 34 out of 40 slides, the

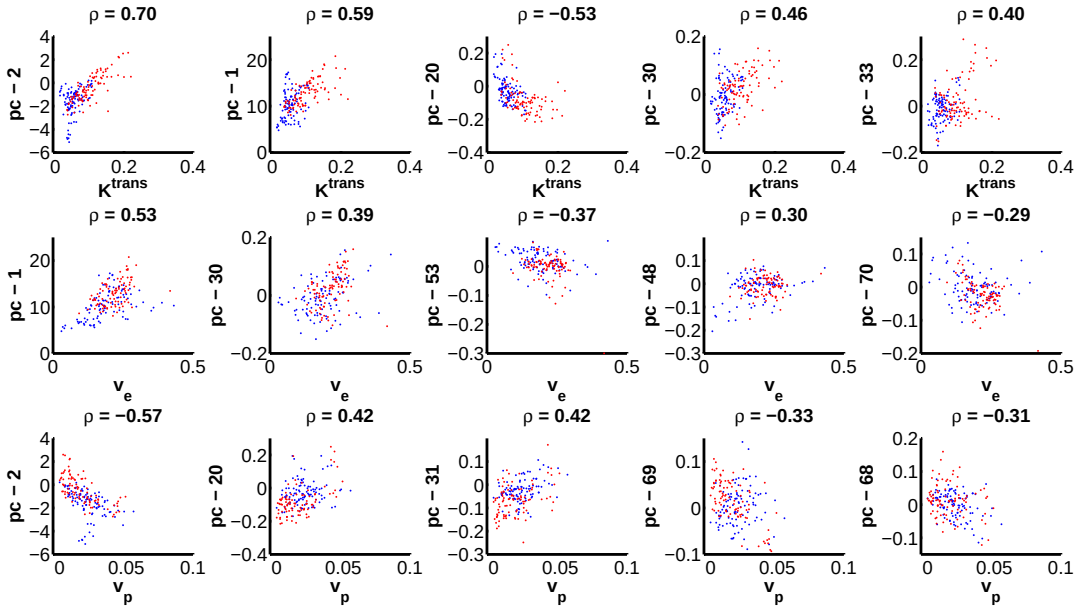

Figure 2. Correlation of principal components (PC) with pharmacokinetic parameters. Red dots are the tumor samples and blue dots are the normal samples. ρ denotes the linear (Pearson) correlation coefficient. For each pharmacokinetic parameters, the five most correlated PCAs are plotted.

Table 1. Area under receiver operating characteristic curve (AUC), sensitivity, specificity and slice-level sensitivity with different feature combinations.

Features	AUC	Sensitivity	Specificity	Slice-level sensitivity
Peripheral Zone Classifier				
Traditional mpMRI Features	0.80 (0.12)	73.9%	73.7%	74.3%
$\langle D \rangle$ and LASSO-PCA Features	0.91 (0.14)	85.9%	80.8%	91.4%
Whole Gland Classifier				
Traditional mpMRI Features	0.68 (0.2)	62.2%	63.5%	60.0%
$\langle D \rangle$ and LASSO-PCA Features	0.87 (0.15)	80.7%	82.0%	85.0%

Table 2. Generated average cancer likelihood values in the format of mean (standard deviation) with different Gleason scores. The likelihood scores were calculated using the peripheral-zone classifier trained on the proposed mpMRI features.

	Normal samples	(3+3) and (3+4) tumors	(3+4+5) and (4+3) tumors
Number of samples	99	77	15
Average cancer likelihood	0.146 (0.19)	0.651 (0.34)	0.780 (0.27)

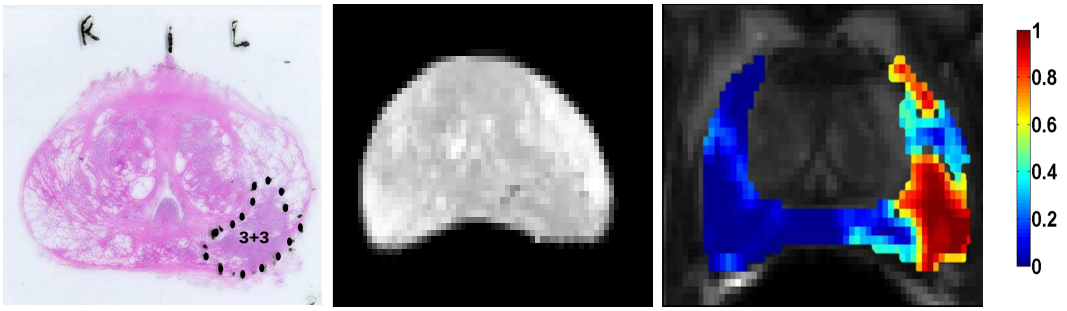

(a) (b) (c)

Figure 3. (a) Peripheral zone tumor marked in pathology slide for one patient. (b) Pathology slide registered to the corresponding T2-weighted image. (c) The generated cancer likelihood map superimposed on the T2-weighted image. Note that the classifier is only trained on the peripheral zone. The classifier is trained on all other cases.

classifier detected more than 50% area of the tumor, and hence the slice-level sensitivity was 85.0%. The statistical significance test between the AUC values with the proposed features and traditional mpMRI features generated a p-value of 0.4. Table 1 summarizes the classifiers' performances.

Correlation of the SVM-based cancer likelihood with Gleason score: We analyzed the cancer likelihood values generated by the peripheral-zone classifier trained on our proposed multiparametric features to find associations with the Gleason score. Table. 2 shows the mean cancer likelihood values with their corresponding Gleason scores. The current dataset does not have any case with a primary or secondary score of 5, but a number of tumors have been marked as 3+4+5, meaning that the pathologist saw a considerable presence of Gleason 5 disease. We grouped the 3+3 and 3+4 tumors together as relatively low risk, and 4+3 with tumors that showed any Gleason score of 5 as high risks. The mean value of cancer likelihood for tumors with Gleason score (3+3) and (3+4) was 0.651, calculated over 77 samples. For more aggressive tumors the average cancer likelihood value was higher than that calculated for less aggressive tumors. We had 15 samples for aggressive tumors with Gleason score (3+4+5) and (4+3), and the mean likelihood value for these samples was 0.78. For normal samples the mean likelihood value was 0.146.

Cancer likelihood maps: We used the classifier trained on the proposed mpMRI features ($\langle D \rangle$ and LASSO-isolated PCA features) to generate cancer likelihood maps for the prostate gland. To generate cancer likelihood maps, the classifier was trained on all other patients and each pixel from the image of interest was used as a test sample for the classifier. To extract the features, each pixel from the T2-weighted MR image was mapped to the corresponding DTI and DCE MR image, and features were extracted from the mapped pixels. The predicted cancer likelihood of the classifier was mapped onto the T2-weighted MRI as a single parameter map of cancer likelihood. Figure 3 shows the cancer likelihood map generated for the peripheral zone of one patient. As can be seen from the image, the finding of the likelihood map is consistent with the pathology image.

We also generated cancer likelihood maps for the entire prostate using the whole gland classifier trained on $\langle D \rangle$ and LASSO-isolated features. Figure 4 shows the cancer likelihood maps for one patient generated for the entire prostate gland. We generated two cancer likelihood maps: one from the mpMRI features and one from the DCE features alone, to observe the effect of registration inaccuracy. As can be seen, the generated cancer likelihood maps detected high likelihood of tumor in the same area where tumor was outlined in the pathology image. However, the tumor region is deformed in the likelihood map generated from mpMRI features. This

(a)

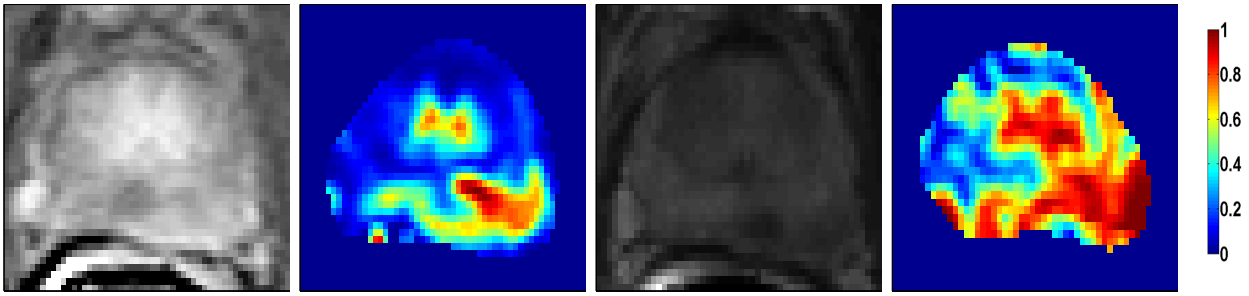

(b) (c) (d) (e)

Figure 4. (a) Peripheral zone tumor marked in pathology slide for one patient. (b) Corresponding DCE image. (c) Cancer likelihood map generated using the classifier trained on data-driven DCE features only. (d) Corresponding T2-weighted image. (e) Cancer likelihood map generated using the classifier trained on the proposed mpMRI features, registered to T2-weighted image.

might be due to the fact that our registration algorithm does not have pixel-level accuracy whereas we used each pixel as an observation to generate the likelihood map. Hence discrepancy is observed between tumor area in cancer likelihood maps generated from mpMRI features and DCE features alone, where no registration was necessary to generate the map. Furthermore, the regions near urethra are erroneously detected as tumor in the whole gland likelihood map. This might be due to the fact that the tissue pattern is different in these regions, and one single classifier for the whole gland might not be the best tool to generate cancer likelihood maps. It might be helpful to train zone-specific classifiers and combine their outcomes to generate whole gland cancer likelihood maps.

4. CONCLUSION

We have developed an image processing pipeline to detect peripheral prostate cancer from mpMRI using data-driven DCE features. We combined diffusion feature with data-driven DCE features and reported and AUC of 0.91 for peripheral-zone classifier, and 0.87 for whole gland classifier. We showed correlation of the generated cancer likelihood scores with their corresponding Gleason scores. Cancer likelihood maps were also generated for the whole prostate gland that showed higher cancer likelihood in cancerous regions. This shows the potential of combining the diffusion MR parameter with the data-driven DCE parameters as an imaging biomarker in prostate cancer diagnosis. The challenge of registration, between DCE and diffusion maps and also to the pathology reference, remains an obstacle in producing pixel-level likelihood maps.

REFERENCES

[1] Barentsz, J. O., Richenberg, J., Clements, R., Choyke, P., Verma, S., Villeirs, G., et al., "ESUR prostate MR guidelines 2012," *European Society of Urogenital Radiology* **22**(4), 746–757 (2012).

[2] Issa, B., "In vivo measurement of the apparent diffusion coefficient in normal and malignant prostatic tissues using echo-planar imaging," *Journal of Magnetic Resonance Imaging* **16**(2), 196–200 (2002).

[3] Yoshizako, T., Wada, A., Uchida, K., Hara, S., Igawa, M., Kitagaki, H., and Maier, S. E., "Apparent diffusion coefficient of line scan diffusion image in normal prostate and prostate cancer-comparison with single-shot echo planner image," *Magnetic resonance imaging* **29**(1), 106–110 (2011).

[4] Gibbs, P., Pickles, M. D., and Turnbull, L. W., "Diffusion imaging of the prostate at 3.0 Tesla," *Investigative Radiology* **41**(2), 185–188 (2006).

[5] Gibbs, P., Liney, G. P., Pickles, M. D., Zelhof, B., Rodrigues, G., and Turnbull, L. W., "Correlation of ADC and T2 measurements with cell density in prostate cancer at 3.0 Tesla," *Investigative Radiology* **44**(9), 572–576 (2009).

[6] Wang, X. Z., Wang, B., Gao, Z. Q., Liu, J. G., Liu, Z. Q., Niu, Q. L., et al., "Diffusion-weighted imaging of prostate cancer: Correlation between apparent diffusion coefficient values and tumor proliferation," *Journal of Magnetic Resonance Imaging* **29**(6), 1360–1366 (2009).

[7] Hambrock, T., Somford, D. M., Huisman, H. J., van Oort, I. M., Witjes, J. A., van de Kaa, H., et al., "Relationship between apparent diffusion coefficients at 3.0-T MR imaging and Gleason grade in peripheral zone prostate cancer," *Radiology* **259**(2), 453–461 (2011).

[8] Tamada, T., Sone, T., Jo, Y., Toshimitsu, S., Yamashita, T., Yamamoto, A., Tanimoto, D., and Ito, K., "Apparent diffusion coefficient values in peripheral and transition zones of the prostate: comparison between normal and malignant prostatic tissues and correlation with histologic grade," *Journal of Magnetic Resonance Imaging* **28**(3), 720–726 (2008).

[9] Manenti, G., Carlani, M., Mancino, S., Colangelo, V., Di Roma, M., Squillaci, E., and Simonetti, G., "Diffusion tensor magnetic resonance imaging of prostate cancer," *Investigative Radiology* **42**(6), 412 – 419 (2007).

[10] Xu, J., Humphrey, P. A., Kibel, A. S., Snyder, A. Z., Narra, V. R., Ackerman, J. J., and Song, S. K., "Magnetic resonance diffusion characteristics of histologically defined prostate cancer in humans," *Magnetic Resonance in Medicine* **61**(4), 842–850 (2009).

[11] Hegde, J. V., Mulkern, R. V., Panych, L. P., Fennessy, F. M., Fedorov, A., Maier, S. E., and Tempany, C., "Multiparametric MRI of prostate cancer: An update on state-of-the-art techniques and their performance in detecting and localizing prostate cancer," *Journal of Magnetic Resonance Imaging* **37**(5), 1035–1054 (2013).

[12] de Rooij, M., Hamoen, E. H. J., Fütterer, J. J., Barentsz, J. O., and Rovers, M. M., "Accuracy of Multiparametric MRI for Prostate Cancer Detection: A Meta-Analysis," *American Journal of Roentgenology* **202**(2), 343–351 (2014).

[13] Oto, A., Kayhan, A., Jiang, Y., Tretiakova, M., Yang, C., Antic, T., et al., "Prostate Cancer: Differentiation of Central Gland Cancer from Benign Prostatic Hyperplasia by Using Diffusion-weighted and Dynamic Contrast-enhanced MR Imaging," *Radiology* **257**(3), 715–723 (2010).

[14] Delongchamps, N. B., Beuvon, F., Eiss, D., Flam, T., Muradyan, N., Zerbib, M., et al., "Multiparametric MRI is helpful to predict tumor focality, stage, and size in patients diagnosed with unilateral low-risk prostate cancer," *Prostate Cancer and Prostatic Diseases* **14**(3), 232–237 (2011).

[15] Langer, D. L., van der Kwast, T. H., Evans, A. J., Trachtenberg, J., Wilson, B. C., and Haider, M. A., "Prostate cancer detection with multi-parametric MRI: Logistic regression analysis of quantitative T2, diffusion-weighted imaging, and dynamic contrast-enhanced MRI," *Journal of Magnetic Resonance Imaging* **30**(2), 327–334 (2009).

[16] Langer, D. L., van der Kwast, T. H., Evans, A. J., Plotkin, A., Trachtenberg, J., Wilson, B. C., and Haider, M. A., "Prostate Tissue Composition and MR Measurements: Investigating the Relationships between ADC, T2, K^{trans}, v_e, and Corresponding Histologic Features," *Radiology* **255**(2), 485–494 (2010).

[17] Ozer, S., Langer, D. L., Liu, X., Haider, M. A., van der Kwast, T. H., Evans, A. J., et al., "Supervised and unsupervised methods for prostate cancer segmentation with multispectral MRI," *Medical Physics* **37**, 1873–1883 (2010).

[18] Kozlowski, P., Chang, S. D., Meng, R., Mädler, B., Bell, R., Jones, E. C., and Goldenberg, S. L., "Combined prostate diffusion tensor imaging and dynamic contrast enhanced MRI at 3T quantitative correlation with biopsy," *Magnetic Resonance Imaging* **28**(5), 621–628 (2010).

[19] Moradi, M., Salcudean, S. E., Chang, S. D., Jones, E. C., Buchan, N., Casey, R. G., et al., "Multiparametric MRI maps for detection and grading of dominant prostate tumors," *Journal of Magnetic Resonance Imaging* **35**(6), 1403–1413 (2012).

[20] Haq, N. F., Kozlowski, P., Jones, E. C., Chang, S. D., Goldenberg, S. L., and Moradi, M., "A data-driven approach to prostate cancer detection from dynamic contrast enhanced MRI," *Computerized Medical Imaging and Graphics* (2014).

[21] Parker, G. J., Suckling, J., Tanner, S. F., Padhani, A. R., Revell, P. B., Husband, J. E., and Leach, M. O., "Probing tumor microvascularity by measurement, analysis and display of contrast agent uptake kinetics," *Journal of Magnetic Resonance Imaging* **7**(3), 564–574 (1997).

[22] Drew, B., Jones, E. C., Reinsberg, S., Yung, A. C., Goldenberg, S. L., and Kozlowski, P., "Device for sectioning prostatectomy specimens to facilitate comparison between histology and in vivo MRI," *Journal of Magnetic Resonance Imaging* **32**(4), 992–996 (2010).